Faraday Discussions

Cite this: *Faraday Discuss.*, 2018, **212**, 399

PAPER

Stereochemistry-dependent hydrogen bonds stabilise stacked conformations in jet-cooled cyclic dipeptides: (LD) *vs.* (LL) cyclo tyrosine–tyrosine†

Feriel BenNasr,[ab] Ariel Pérez-Mellor,[a] Ivan Alata,[a] Valeria Lepere,[a] Nejm-Eddine Jaïdane[b] and Anne Zehnacker *[a]

Received 22nd April 2018, Accepted 6th June 2018
DOI: 10.1039/c8fd00079d

Tyrosine-containing cyclic dipeptides based on a diketopiperazine (DKP) ring are studied under jet-cooled conditions using resonance-enhanced multi-photon ionisation (REMPI), conformer-selective IR-UV double resonance vibrational spectroscopy and quantum chemical calculations. The conformational landscape of the dipeptide containing natural L tyrosine (Tyr), namely c-LTyr–LTyr strongly differs from that of its diastereomer c-LTyr–DTyr. A similar family of conformers exists in both systems, with one aromatic ring folded on the dipeptide DKP ring and the other one extended. Weak NH$\cdots\pi$ and CH$\cdots\pi$ interactions are observed, which are slightly different in c-LTyr–LTyr and c-LTyr–DTyr. These structures are identical to those of LL and LD cyclo diphenylalanine, which only differ from c-Tyr–Tyr by the absence of hydroxyl on the benzene rings. While this is the only conformation observed for c-LTyr–DTyr, c-LTyr–LTyr exhibits an additional form stabilised by the interaction of the two hydroxyls, in which the two aromatic rings are in a stacked geometry. Stereochemical effects are still visible in the radical cation, for which one structure is observed for c-LTyr–DTyr, while the spectrum of the c-LTyr–LTyr radical cation is explained in terms of two co-existing structures.

I. Introduction

Peptides are characterised by well-defined secondary structures, such as helices or turns. They are stabilised by a delicate balance between non-covalent interactions, either localised on a well-defined part of the molecule like hydrogen bonds, or more delocalised in nature, like dispersion between aromatic rings.

[a]*Institut des Sciences Moléculaires d'Orsay (ISMO), CNRS, Univ. Paris-Sud, Université Paris-Saclay, F-91405 Orsay, France. E-mail: anne.zehnacker-rentien@u-psud.fr*
[b]*Laboratoire de Spectroscopie Atomique, Moléculaire et Applications (LSAMA), Université de Tunis El Manar, Tunis 1060, Tunisia*

† Electronic supplementary information (ESI) available. See DOI: 10.1039/c8fd00079d

Laser spectroscopy experiments of small neutral peptides isolated in the gas phase have been conducted in the past decade to probe their conformational flexibility without the perturbation brought upon by the solvent.[1–3] In particular, numerous jet-cooled peptides have been characterized using conformer-selective experiments, like α peptides[4–6] or artificial β or γ peptides,[7–10] as well as cyclic peptides[11–13] or biomimetic systems.[14]

Among the non-covalent interactions shaping the biopolymers, hydrogen bonds are especially interesting due to their ubiquity and diversity. They include strong OH···O, OH···N, NH···O or NH···S hydrogen bonds, mainly stabilised by electrostatic forces, but also those involving an aromatic ring like NH···π, OH···π, and CH···π.[15–23] Amide stacking also influences the shape of small peptides.[24] These interactions are weaker than conventional hydrogen bonds and dispersion strongly contributes to them.

Dispersion is especially important for peptides containing aromatic residues. It influences the folding propensity[25] and is responsible for the formation of hydrophobic domains in peptides.[26,27] Aromatic–aromatic interaction has been studied in neutral peptides containing several phenylalanine (Phe) chromophores.[28–30] The presence of aromatic rings also influences the structure of Phe-containing protonated or cationised peptides by acting as a hydrogen bond acceptor or interacting with the cation.[31,32]

However, the theoretical description of the competition between dispersion and electrostatics is still a challenge. This has prompted numerous studies of gas-phase model systems.[16,25,33–35] The balance between hydrogen bonds and dispersion is very delicate and is influenced by several factors like substitution, solvation, or even chirality as observed in the dimer of 1-indanol.[34] The influence of stereochemistry on the structure of biomolecules has been studied in alkaloids,[36,37] lignin subunits,[38] or model cyclic systems.[39–41] The structural consequences of the chirality of the residues have been studied on examples of α-peptides like valine–phenylalanine and phenylalanine–phenylalanine[28] or capped phenylalanine–alanine[42] but also in non-natural β- or γ-peptides.[7,8,43,44] Aromatic–aromatic interactions have been shown to play an important role in defining the NH stretching frequencies in capped Phe–Phe diastereomers.[29]

Cyclic dipeptides, also known as diketopiperazine (DKP) peptides, attract much attention because of their potential pharmacological activity,[45,46] in particular, those comprising an aromatic residue because aromatic rings are often involved in the interaction with the receptor.[47] Most of the previous studies have been conducted in the condensed phase, although a few gas-phase studies have been reported.[30,48,49] The structure strongly depends on the nature of the substituents. The DKP ring itself, as a six-membered ring, can adopt many conformations. While it is planar (P) for small substituents, as in cyclo Gly–Gly,[50] it adopts an out-of-plane conformation for bulkier substituents. It is, for example, boat (B) in cyclo LAla–LAla,[51] or chair (C) for cyclo Tyr–Pro.[52] Of special interest are the DKP dipeptides containing identical residues. Various groups of symmetry are encountered in these systems. Cyclo DAla–LAla shows C_i symmetry, because of the planarity of the DKP ring and the equivalent positions of the two CH_3 substituents.[53] Dissymmetry can be brought about by the interaction between the two residues, as exemplified by cyclo Phe–Phe.[30,49,54] We have recently studied the effects of chirality on the shape of cyclo Phe–Phe.[30] This molecule shows only one conformer under jet-cooled conditions. The two Phe are in different positions;

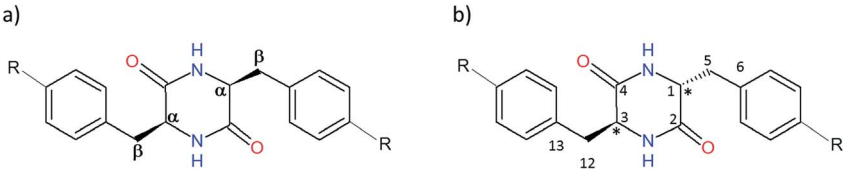

Fig. 1 Scheme of the molecules under study, with atom numbering. R = H for phenylalanine or R = OH for tyrosine. The chiral centres are indicated by * in c-LD. (a) Homochiral dipeptide c-LL. (b) Heterochiral dipeptide c-LD.

one is folded over the DKP ring in a flagpole position, while the other one is extended, which allows a stabilising CH$\cdots\pi$ interaction to take place. Cyclo LPhe–LPhe and cyclo LPhe–DPhe only slightly differ from each other, by the nature of the CH$\cdots\pi$ interaction and by the strength of a secondary NH$\cdots\pi$ interaction, which results in spectroscopic differences in the ν(NH) stretching region.

Here, we extend this study to cyclo Tyr–Tyr (Fig. 1). The reason for choosing this system is that it differs from cyclo Phe–Phe (see Fig. 1) by the presence of OH substituents on the aromatic rings. Additional interactions such as OH$\cdots$O or OH$\cdots\pi$ hydrogen bonds are therefore expected. Only the natural form LL has been studied so far in the condensed phase. Cyclo Tyr–Tyr has been studied in different solvents using NMR spectroscopy.[55] Although the NMR spectra did not provide a direct conclusion as to its structure, it seems that a folded conformation can be ruled out. Electronic circular dichroism combined with molecular dynamics simulations has suggested that several conformers exist in water solutions, ranging to structures with almost parallel rings to fully extended structures.[56] However, the solvent, water in this case, may strongly modify the structure relative to the gas phase.

Here we apply conformer-selective IR-UV double resonance vibrational spectroscopy to the structural study of cyclo LTyr–LTyr and cyclo LTyr–DTyr under jet-cooled conditions. Quantum chemical calculations are conducted to assist in the interpretation of the experimental findings. We extend this study to the radical cation form of cyclo Tyr–Tyr. The obtained results are compared to the previously studied cyclo Phe–Phe system, which allows assessment of the influence of aromatic-ring substitution in shaping the structure of DKP-base dipeptides.[30]

II. Experimental and theoretical methods

II-(A) Experimental methods

Cyclo Tyr–Tyr (>99%) was purchased from Novopep Limited (Shanghai - China) and used without further purification. The experimental set-up has already been described in detail.[36] Briefly, the dipeptides were put into the gas phase using a homemade laser desorption source.[57] A few mg of the sample mixed with a carbon matrix was fixed on a linear translation system. The species were desorbed by the second harmonic of a Nd:YAG laser (Continuum Minilite) propagated by an optical fibre to the surface of the carbon bar. The pulsed supersonic expansion was generated by expanding argon ($\sim$4 bar) through a 300 μm nozzle (General Valve Parker) into a vacuum chamber. Mass-resolved S_0–S_1 spectra were obtained using one-colour resonance-enhanced two-photon ionisation (RE2PI)

spectroscopy. The ions were mass-selected by a linear time-of-flight mass spectrometer (Jordan, one-meter length) and detected using a microchannel plate (RM Jordan, 25 mm diameter). The ion signal was averaged using an oscilloscope (Lecroy WaveSurfer) and processed through a personal computer.

Vibrational spectra were obtained using the IR-UV double resonance technique.[18,58,59] Two synchronized laser beams were co-focused in the cold region of the supersonic expansion. The UV probe was fixed on each main vibronic band of the S_0–S_1 transition, while the IR pump was scanned in the region of interest. Absorption of the IR photons was measured as a dip in the probe-induced ion current, allowing for the measurement of mass-resolved conformer-selective vibrational IR spectra.

The UV laser (0.02 cm^{-1} resolution) was a frequency-doubled dye laser (Sirah equipped with C540 A dye) pumped by the second harmonic of a Nd:YAG laser (Quanta-Ray, Spectra-Physics). The IR source (3 cm^{-1} resolution) was an optical parametric oscillator/amplifier (OPO/OPA) (Laser Vision). The IR pulse was triggered 80 ns before the UV pulse for recording the IR spectrum of the neutral molecules in their electronic ground state and 50 ns after for the ion. It was focused by a 0.5 m focal length lens. A homemade gate generator controlled the synchronization between the lasers. A homemade active baseline subtraction scheme was used to monitor the IR absorption as the difference in ion signal produced by successive UV laser pulses (one without and one with the IR laser).

II-(B) Theoretical methods

The potential energy surface of c-LTyr–LTyr and c-LTyr–DTyr were manually explored, starting from the six local minima obtained for cyclo Phe–Phe, *vide infra*. The corresponding structures were optimised using the B3LYP functional combined to the 6-311++G(d,p) basis set and including D3 empirical corrections for dispersion.[60–62] This level of theory was chosen because it satisfactorily reproduces the vibrational frequencies of similar systems with an acceptable calculation cost.[30,32,49] The charge distribution was obtained from the Natural Bond Orbital (NBO) analysis.[63]

The harmonic vibrational frequencies were calculated at the same level of theory and the absence of imaginary frequencies checked for all local minima. The vibrational spectra were simulated by convoluting the harmonic frequencies obtained thereby by a Lorentzian line shape (FWHM 4 cm^{-1}). The harmonic frequencies were scaled by 0.952 to account for anharmonicity and basis set incompleteness. All calculations were performed with the Gaussian package.[64]

The electronic excited state energies were calculated using the time-dependent DFT (TD-DFT) method. The level of theory employed was ωB97XD/aug-cc-pVDZ, which has shown to satisfactorily describe the electronic excited states.[65–66] The calculations were limited to the structural families experimentally observed, *vide infra*. The vertical excitation energies were computed for the first ten singlet excited states. The vertical ionization energy was calculated at the same level of theory.

The intramolecular interactions were visualized by means of the Non-Covalent Interaction (NCI) technique.[67] This method and its application to intramolecular H-bonds has been described previously in detail.[67–69] Briefly, the NCI technique rests on a topological analysis of the electron density ρ and its reduced gradient

$s(\rho)$ in regions of weak electron density and small reduced gradient. Non-covalent interactions correspond to zones where $s(\rho)$ vanishes, *i.e.* ρ is close to a minimum. The visualization was accomplished by plotting iso-surfaces of the reduced gradient with a RGB colouring scheme resting on the sign of the second eigenvalue, λ_2, of the Hessian matrix. Red iso-surfaces correspond to positive λ_2, *i.e.* repulsive regions and blue iso-surfaces correspond to negative λ_2, *i.e.* regions corresponding to favourable interactions. Green iso-surfaces correspond to weak delocalised interactions, *i.e.* regions where λ_2 is close to zero. The NCI calculations used electronic density obtained from the Gaussian.wfn output file at the same level of theory as the geometry optimisation. A cut-off of 0.35 was used. The 3-D NCI images were plotted using the VMD software.[70]

III. Results and discussion

III-(A) Calculated structures

(a) Nomenclature. The parameters that describe the geometry of cyclo Tyr–Tyr are shown in Fig. 1 and 2. The orientation of each aromatic substituent is described relative to the corresponding amide bond. Three geometries are possible, namely, two *gauche* geometries, g^+ and g^-, and one *trans* t, as shown in Fig. 2a. They correspond to dihedral angles τ_1 (N C_1 C_5 C_6) and τ_2 (N C_3 C_{12} C_{13}) of about 60°, −60°, 180° for the L residue, respectively, while the sign of the angles is the opposite for the D residue. Lastly, two orientations relative to the DKP ring, **I** and **II**, are possible for the tyrosine hydroxyls, which leads to four isomers for each DKP ring geometry and substituent orientation. They are defined in Fig. 2b. In what follows, we shall denote the cyclic nature of the peptide by "c-", followed by their geometry g^+, g^-, or t. L or D configurations, *i.e.* *S* or *R* chirality, respectively, in the Cahn–Ingold–Prelog nomenclature, are denoted by L or D in subscript, followed by the **I** or **II** positions of the tyrosyl OH.

(b) Neutral ground state. The calculated structures of c-LL can be classified into six groups corresponding to the combination of the g^+, g^-, and t positions of the aromatic substituents. Each group comprises four structures close in energy (within ~0.3–0.7 kcal mol^{-1}), which correspond to the four possible orientations **I** and **II** of the hydroxyl groups. However, for c-LL structures of C_2 symmetry, some

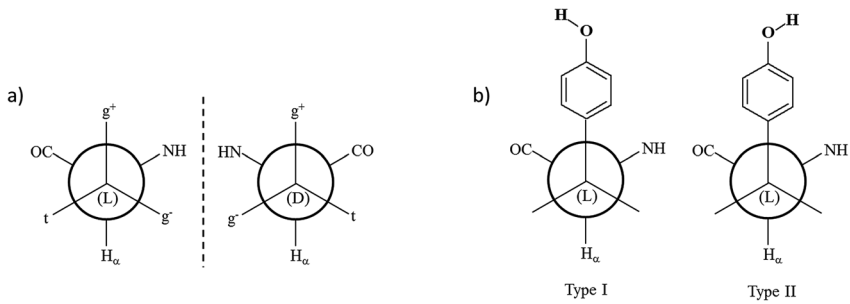

Fig. 2 (a) Aromatic ring positions in cyclo Tyr–Tyr that correspond to g^+, g^-, and t conformations for a L Tyr residue (left) and D Tyr residue (right). (b) Definition of the two positions of the hydroxyl substituent: for each position of the tyrosine residue (g^+, g^-, t), the hydroxyl group is directed anticlockwise (type I) or clockwise (type II).

of these geometries are equivalent (see Table S1 in the ESI†). Previous studies of the amino acid tyrosine have shown its high flexibility. Up to 12 conformers have been observed.[71,72] Those corresponding to the rotation of the hydroxyl substituent could not be discriminated by their IR spectra and UV-UV double resonance spectroscopy was necessary to distinguish them.[72] In the systems studied here, there is no means of distinguishing the four OH possible orientations and we will discuss the structures in terms of families that include the four OH orientations. The most stable calculated structures of each family are shown in Fig. 3 and the corresponding structural parameters and energies are listed in Table 1. The other conformers of each family are not shown because they only differ by the rotation of the OH groups. The complete set of energetic data is given in Table S1 in the ESI.†

The results listed in Table 1 indicate that most of the population of c-LD (~80%) belongs to one family, namely c-$g_L^+g_D^-$. In contrast, the population of c-LL is spread over two families, c-$g_L^+g_L^-$, (~60%) and c-$g_L^+g_L^+$, (~35%). The other families exist as minor contributions. The most stable c-LL family, exemplified by c-$g_{LII}^+g_{LI}^-$, is identical to the most stable structure observed for cyclic diphenylalanine, cyclo LPhe–LPhe.[30] One of the aromatic rings g_L^- is extended out of the dipeptide ring, while the other one, g_L^+, is folded over it. As a result, the two aromatic rings are far from each other (5.56 Å between their centres). In particular, the two OH groups do not interact at all. Weak $C_\beta H\cdots\pi$ and $NH\cdots\pi$ interactions contribute to the stability of the system.

The geometry of the second most stable c-LL family, epitomised by $g_{LI}^+g_{LI}^+$, is completely different. The two aromatic rings are in equivalent positions and facing each other, which allows interaction between the two hydroxyls. The relative Gibbs energy of $g_{LI}^+g_{LI}^+$ is only 0.2 kcal mol^{-1}. This contrasts with cyclo LPhe–LPhe, in which the structure with benzene in a stacked position is calculated at 3 kcal mol^{-1} higher in energy than the most stable form.[30] Dispersion between the benzene rings is the only stabilising interaction in cyclo LPhe–LPhe and cannot counterbalance the expected repulsion, in contrast with cyclo LTyr–LTyr where a hydrogen bond is formed. However, the hydrogen bond is not

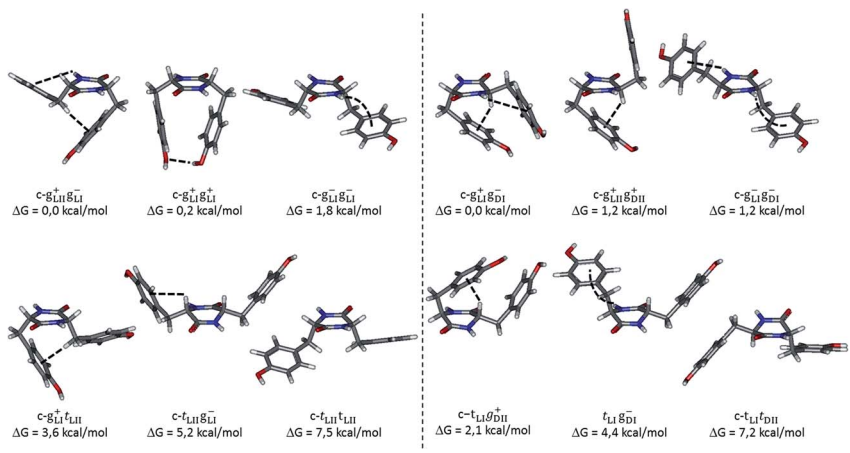

Fig. 3 Most stable calculated structures for each family of cyclo Tyr–Tyr. c-LL (left) and c-LD (right).

Table 1 Energetic and structural parameters of the most stable calculated conformer of each family for cyclo LTyr–LTyr (c-LL) and cyclo LTyr–DTyr (c-LD). (*) The energy difference of the most stable structure of cyclo LTyr–DTyr relative to the most stable structure of cyclo LTyr–LTyr is given in parentheses

Structure family c-LL	Representative example	Electronic energy, ΔE (kcal mol^{-1})	ZPE-corrected electronic energy, ΔE_{ZPE} (kcal mol^{-1})	Gibbs free energy, ΔG (kcal mol^{-1})	Population (%)	Distance between the centres of the aromatic rings (Å)	Shortest OH···O distance (Å)	CH···π distance (Å)	NH···π distance (Å)
c-$g_L^+g_L^-$	c-$g_{LII}^+g_{LI}^-$	1.6	1.2	0.0	61	5.56	7.61	2.52 (C_β)	3.30
c-$g_L^+g_L^+$	c-$g_{LI}^+g_{LI}^+$	0.6	0.3	0.2	35	4.09	2.23	>4	>4
c-$g_L^-g_L^-$	c-$g_{LI}^-g_{LI}^-$	5.1	4.4	1.8	3	8.92	14.31	>4	3.37 (3.37)
c-$g_L^+t_L$	c-$g_{LI}^+t_{LII}$	5.7	5.0	3.6	<1	5.51	7.29	2.49 (C_β)	>4
c-$t_Lg_L^-$	c-$t_{LII}g_{LI}^-$	9.2	8.0	5.2	0.0	9.26	12.66	>4	3.26
c-t_Lt_L	c-$t_{LII}t_{LII}$	12.2	10.8	7.5	0.0	8.87	14.31	>4	>4

Structure family c-LD	Representative example	Electronic energy, ΔE (kcal mol^{-1})	ZPE-corrected electronic energy, ΔE_{ZPE} (kcal mol^{-1})	Gibbs free energy, ΔG (kcal mol^{-1})	Population (%)	Distance between the centres of the aromatic rings (Å)	Shortest OH···O distance (Å)	CH···π distance (Å)	NH···π distance (Å)
c-$g_L^+g_D^-$	c-$g_{LI}^+g_{DI}^-$	0.0 (2.0)*	0.0 (1.5)*	0.0 (0.5)*	78	5.15	5.02	2.40 (C_α)	3.35
c-$g_L^+g_D^+$	c-$g_{LII}^+g_{DI}^+$	1.9	1.7	1.2	11	7.35	11.45	2.70 (C_α)	>4
c-$g_L^-g_D^-$	c-$g_{LI}^-g_{DII}^-$	3.6	3.2	1.2	10	9.62	14.83	>4	3.25 (3.36)
c-$t_Lg_D^+$	c-$t_{LI}g_{DII}^+$	1.7	1.8	2.1	1	4.40	2.77	2.41 (C_α)	>4
c-$t_Lg_D^-$	c-$t_{LI}g_{DI}^-$	7.1	6.6	4.4	<1	8.32	11.44	>4	3.5
c-t_Lt_D	c-$t_{LI}t_{DII}$	10.0	9.1	7.2	0.0	8.91	13.93	>4	>4

optimal (OH···O distance of 2.23 Å) in $g_{LI}^{+}g_{LI}^{+}$, and is far from linear (OH···O angle of 128°). The two OH groups have their dipole oriented in an antiparallel manner and strong dipole–dipole interaction probably also contributes to the stabilisation. This is reminiscent of the stabilisation due to amide stacking in γ-peptides.[24] In the present case, the formation of a stronger OH···O hydrogen bond is prevented, not by steric constraints as in γ-peptides, but by the necessary out-of-plane distortion of the hydroxyl that results in a loss in conjugation between the oxygen lone pair and the aromatic ring. Calculations yield a similar form c-$g_{LI}^{+}g_{LII}^{+}$, which is not the most stable c-$g_{L}^{+}g_{L}^{+}$ form in terms of Gibbs energy, but it is the most stable in terms of electronic energy. Its only structural difference relative to c-$g_{LI}^{+}g_{LI}^{+}$ shown in Fig. 3 is that the two OH groups are pointing in the same direction, while they are pointing towards each other in c-$g_{LI}^{+}g_{LI}^{+}$. This OH orientation in c-$g_{LI}^{+}g_{LII}^{+}$ allows optimisation of the OH···O hydrogen bond (OH···O distance of 2.01 Å and O$\hat{H}$O angle of 153°). As will be seen later, c-$g_{LI}^{+}g_{LII}^{+}$ reproduces the experimental results better than c-$g_{LI}^{+}g_{LI}^{+}$; for this reason we will focus on the former in what follows. In c-$g_{LI}^{+}g_{LII}^{+}$, the two peptide bonds are planar and the two planes make an angle of 15°, resulting in a V-shaped DKP ring, with the aromatic rings located on the top of the V.

The other minima found in the calculations lie more than ∼1.8 kcal mol^{-1} higher in energy than the most stable form and will not be discussed further.

It should be stressed at this stage that the four c-$g_{L}^{+}g_{L}^{-}$ conformers are close in energy, within 0.3 kcal mol^{-1}. They are probably all populated in our experimental conditions, as are the conformers of tyrosine with different OH orientations.[71,72]

c-LD possesses two substituents of identical chemical nature but of opposite configurations; as a result, the calculated structures consist of pairs of non-superimposable mirror images. Notwithstanding this property, the results obtained for c-LD parallel those for c-LL and the calculated structures can also be divided into six families, with similar energy orders. The most stable conformer is of identical nature for the two stereomers. In c-$g_{L}^{+}g_{D}^{-}$, the g_{L}^{+} residue is in a pseudo-axial position; it is folded over the DKP ring and acts as an acceptor in the $C_{\alpha}H\cdots\pi$ interaction. The g_{D}^{-} residue is in a pseudo-equatorial position and is extended.

The major difference between c-$g_{L}^{+}g_{D}^{-}$ and c-$g_{L}^{+}g_{L}^{-}$ is the nature of the CH···π interaction, as already described for the non-substituted cyclo Phe–Phe dipeptide. Because of the difference in geometry (axial for g_{L}^{-} and equatorial for g_{D}^{-}) between the diastereomers, the CH···π hydrogen bond involves $C_{\alpha}H$ as a donor in c-$g_{L}^{+}g_{D}^{-}$ *vs.* $C_{\beta}H$ in c-$g_{L}^{+}g_{L}^{-}$. The two diastereomers c-LL and c-LD also differ in the energy ordering of the different families. The c-$g^{+}g^{-}$ and c-$g^{+}g^{+}$ families are almost iso-energetic in c-LL but separated by more than 1 kcal mol^{-1} in c-LD. This is because the two aromatic rings, both in equatorial positions in c-LL, are in axial/equatorial position in c-LD, which does not allow hydrogen bond formation in c-$g_{L}^{+}g_{D}^{+}$. The only structure with parallel orientation of the aromatic rings is c-$t_{LI}g_{DII}^{+}$, which lies however more than 2 kcal mol^{-1} higher in energy. In this structure, the OH···O distance is larger than expected for a hydrogen bond (2.77 Å), because of the steric constraints due to the DKP ring. Indeed, it is not possible to have proper interaction between the two OH groups when one residue is in pseudo axial position and the other one in pseudo equatorial position as it is in c-LD. c-LD and c-LL also differ by the geometry of the DKP ring. In both cases, the

peptide bond is not planar and the amide nitrogens are located opposite to the carbons in α relative to the mean plane of the molecule. However, the out-of-plane distortion of the DKP ring is more pronounced in c-LD.

We can conclude from these calculations that only conformers belonging to the most stable family c-g^+g^- will be observed for c-LD, while an additional c-g^+g^+ conformer should be populated in c-LL.

Fig. 4 shows the NCI plots obtained for the stable structures of c-LL and c-LD, which are used for the assignment, *vide infra*. The NCI plot of the c-LL hydrogen-bonded structure c-$g_{LI}{}^+g_{LII}{}^+$ shows a very strong OH$\cdots$O interaction, evidenced by a deep blue pellet and corresponding to a high electron density value (0.015 a.u.) at the critical point. Two bicolour pellets characteristic of intramolecular hydrogen bonding from $C_\beta H$ to the adjacent amide O=C are also visible, with notable critical densities (0.096 a.u.). The NCI plots of the conformations that the two diastereomers have in common, namely, c-$g_{LII}{}^+g_{LI}{}^-$ and c-$g_{LI}{}^+g_{DI}{}^-$, are similar. They both show the CH$\cdots$O interaction already mentioned for the hydrogen-bonded structure, with similar critical electron densities (0.0090 for c-LL and 0.0096 for c-LD). The NH$\cdots\pi$ interaction is slightly weaker in c-LL than c-LD with a critical electron density of 0.0071 and 0.0078, respectively. A green-yellowish pellet is also seen in both cases, which corresponds to the CH$\cdots\pi$ interaction, which is slightly stronger in c-LD ($C_\alpha H\cdots\pi$) with a critical electron density of 0.0062 *vs.* 0.058 for c-LL ($C_\beta H\cdots\pi$). This parallels what has been observed in the related cyclo Phe–Phe system.[30]

(c) Electronic excited state. The presence of two chromophores raises the question of the localisation of the electronic excitation. The energy and the transition dipole moment of the first ten electronic transitions are summarised in Fig. 5 for the structures used for the assignment. We will limit the discussion to the first two electronic transitions in what follows, because S_{3-10} are higher in energy by at least 1000 cm^{-1}; they are therefore out of our experimental range. The family that the two diastereomers have in common, namely, c-g^+g^-, displays a similar pattern for the two diastereomers. The electronic transition energy does not depend much on the orientation of the OH groups, which is not surprising as they show no interaction with the rest of the molecule. The case of the hydrogen-bonded family c-$g_L{}^+g_L{}^+$ is different. The energy of the first electronic transition is much lower for the hydrogen-bonded form c-$g_{LI}{}^+g_{LII}{}^+$. The S_1 transition (Fig. 6) is a $\pi\pi^*$ transition localised on the ring acting as a hydrogen bond donor while the S_2 transition is the $\pi\pi^*$ transition of the acceptor part. In the other conformers, the S_1 and S_2 transitions are well localised too and correspond to the $\pi\pi^*$

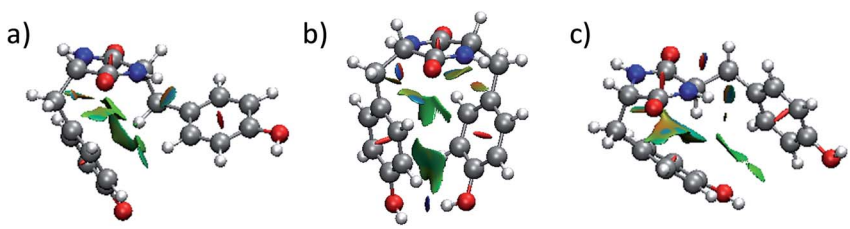

Fig. 4 NCI plot of the experimentally observed structures with red pellets corresponding to repulsive regions, blue to favourable interactions and green to weak delocalised interactions: (a) c-$g_{LII}{}^+g_{LI}{}^-$, (b) c-$g_{LI}{}^+g_{LII}{}^+$ and (c) c-$g_{LI}{}^+g_{DI}{}^-$.

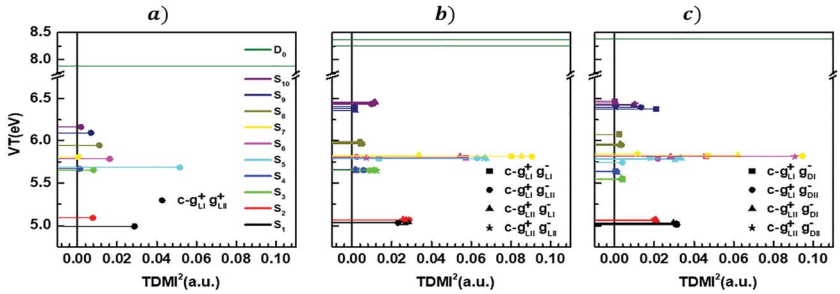

Fig. 5 Vertical transition energies of the, (a) c-$g_L^+g_L^+$, (b) c-$g_l^+g_L^-$ and (c) c-$g_L^+g_D^-$ families. The transition dipole moment integral is given as the length of the horizontal bar. The colour code denotes the electronic transitions $S_0 \rightarrow S_i$ ($i = 1 \ldots 10$) and the ionisation $S_0 \rightarrow D_0$. Each geometry of a given family is discriminated by square (■), triangle (▲), circle (●), and star (★). For the sake of clarity, the zero of the transition dipole moment integral is shifted and denoted by a vertical black line.

transitions localised on the extended (for S_1) and folded (for S_2) aromatic rings. These results point out the different nature of the hydrogen-bonded complex.

(d) Ionic state. The radical cations of c-LL and c-LD are optimised at the same level of theory as the neutral forms. As the radical cation is formed by photoionisation, it is expected that the initial geometry is that of the neutral form, which then relaxes further. For this reason, the structures of the neutral forms used for the assignment have been taken as starting geometries for the optimisation (*vide infra*). The obtained structures are shown in Fig. 7 and the corresponding structural parameters are listed in Table 2. Optimisation of the ion obtained by removing an electron from the most stable neutral form of c-LL (c-$g_{LII}^+g_{LI}^-$) results in c_{ion}-$g_{LII}^+t_{LII}$ with dihedral angles τ of 63 and −176°. It should be noted that the g_{LI}^- aromatic ring is fully extended in the neutral form, which favours the NH$\cdots\pi$ interaction. In the ion, it undergoes a rotation that favours a stabilising interaction between the amide CO and the aromatic ring. Optimisation of the cation resulting from the ionisation of the other conformer (c-$g_{LI}^+g_{LII}^+$) results in c_{ion}-$g_{LI}^+g_{LII}^+$, with dihedral angles of 56 and 57°. The energy order is reverted in the ion relative to the neutral form and the hydrogen-bonded form c-$g_{LI}^+g_{LII}^+$ is 2.7 kcal mol^{-1} more stable in the ion. The DKP ring geometry is not much modified upon ionisation, in both structures.

The structure obtained when optimising the ion resulting from the vertical ionisation of the most stable c-LD (c-$g_{LI}^+g_{DI}^-$) is c_{ion}-$g_{LI}^+t_{DI}$, with dihedral angles τ of 60 and −177°. The main difference relative to the neutral form is that the g^- conformation is not stable and evolves to a t conformation, as described above for c-LL.

NBO analysis allows assessment of the charge localisation in the ions. The NBO charge distribution is very dissymmetrical, and the two rings strongly differ from each other in terms of electron density. In c_{ion}-$g_{LI}^+t_{DI}$, most of the charge (0.692) is localised on the extended g_{LI}^+ moiety, while the charge on the t_{DI} subunit, which is folded on the DKP ring, is close to zero (0.028). Then, the ν(OH) stretching frequency of the folded aromatic ring should not be shifted relative to the neutral form. The rest of the charge is borne by the DKP ring, mainly the $C_\alpha H$

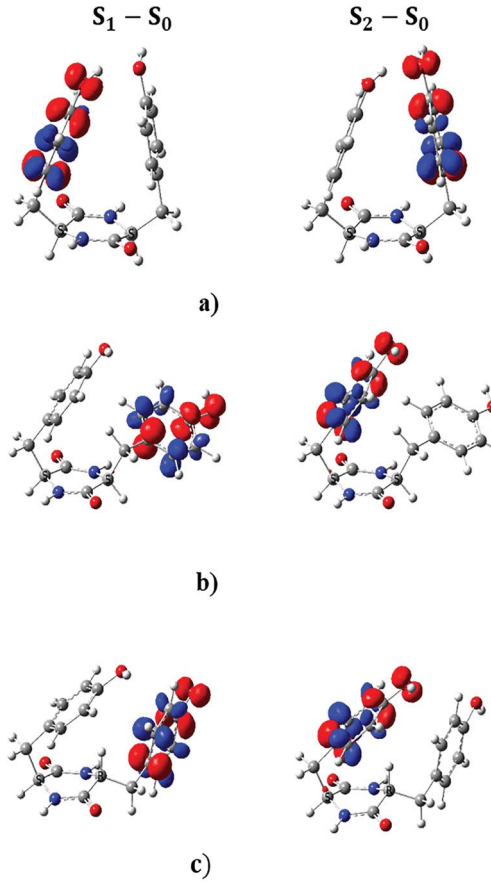

Fig. 6 Difference in electron density between the S_1 and S_2 electronic excited states relative to the ground state S_0, for the structures used for the assignment. (a) c-$g_{LI}^{+}g_{LII}^{+}$, (b) c-$g_{LII}^{+}g_{LI}^{-}$ and (c) c-$g_{LI}^{+}g_{DI}^{-}$. The electron density isovalue is 0.004 a.u. The sign of the electron density difference is coded in blue for positive and red for negative.

groups (0.148 for $C_\alpha H$ in interaction with the folded aromatic ring and 0.159 for the other). The $C_\beta H_2$ groups have limited charge, namely 0.065 (folded) and 0.069 (extended), as do the two peptide bonds HNCO (0.03). Similar results are obtained for c_{ion}-$g_{LII}^{+}t_{LII}$. Most of the charge is borne by the extended aromatic ring (0.629), the charge of the folded ring being much less (0.136). Also the hydrogen-bonded structure c-$g_{LI}^{+}g_{LII}^{+}$ shows a dissymmetric distribution of the charge; the charge of the H-bond donor is 0.654 *vs.* 0.232 for the acceptor. Thus, the ν(OH) stretching frequency of the acceptor aromatic ring should be less shifted relative to the neutral form than that of the donor. We can conclude from these results that the two rings are not equivalent in the ion, which should be reflected in their vibrational spectra.

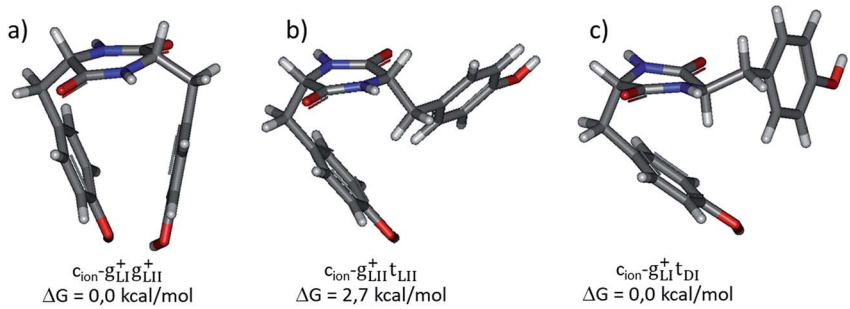

Fig. 7 Calculated structures of the cyclo Tyr–Tyr cation of c-LL (a) c_{ion}-$g_{LI}{}^{+}g_{LII}{}^{+}$, (b) c_{ion}-$g_{LII}{}^{+}t_{LII}$ and c-LD (c) c_{ion}-$g_{LI}{}^{+}t_{DI}$.

Table 2 Structural parameters of the ions obtained by ionisation of the most stable calculated conformers of cyclo LTyr–DTyr and cyclo LTyr–LTyr

Representative example	Gibbs free energy, ΔG (kcal mol^{-1})	Distance between the centres of the aromatic rings (Å)	Shortest OH···O distance (Å)	CH···π distance (Å)	NH···π distance (Å)
c_{ion}-$g_{LI}{}^{+}g_{LII}{}^{+}$	0	3.91	1.94	>4	>4
c_{ion}-$g_{LII}{}^{+}t_{LII}$	2.7	5.50	7.26	2.63 (C_β)	>4
c_{ion}-$g_{LI}{}^{+}t_{DI}$	—	5.54	6.26	2.45 (C_α)	>4

III-(B) Experimental results

(a) Electronic spectroscopy. The 1c-RE2PI spectra of c-LL and c-LD are shown in Fig. 8. The two diastereomers have in common a broad absorption showing two maxima, located at ~35 600 and 35 800 cm^{-1} for c-LL *vs.* 35 500 and 35 800 cm^{-1} for c-LD. Narrow lines are superimposed on the broad absorption for c-LL, with an origin at 35 274 cm^{-1}, while c-LD only shows the broad absorption. Insufficient cooling of the sample could be responsible for the broad absorption and the absence of resolved transitions in c-LD. To test this hypothesis, we have simultaneously introduced carbon pellets containing each of the two diastereomers in the set-up and recorded their spectra successively in exactly the same experimental conditions. The spectra remain identical, which shows that the different spectroscopic properties of c-LL and c-LD are not due to different experimental conditions. Two hypotheses might explain the width of the c-LD spectrum. The first one is that fast non-radiative processes happen in the electronic excited state. However, tyrosine as well as protonated tyrosine show well separated bands under supersonic expansion or cryogenic ion trap conditions, which indicates lifetimes on the order of nanoseconds.[72–74] Another possibility would be spectral congestion and insufficient cooling of the studied molecules. Indeed, as we shall see later, only one member of a structural family can explain the narrow spectrum obtained for c-LL, while several members of another family can explain the broad spectrum, for c-LL and c-LD alike. Therefore, it is possible that the spectral width is due to the superposition of the absorption of several conformers belonging to the same family.

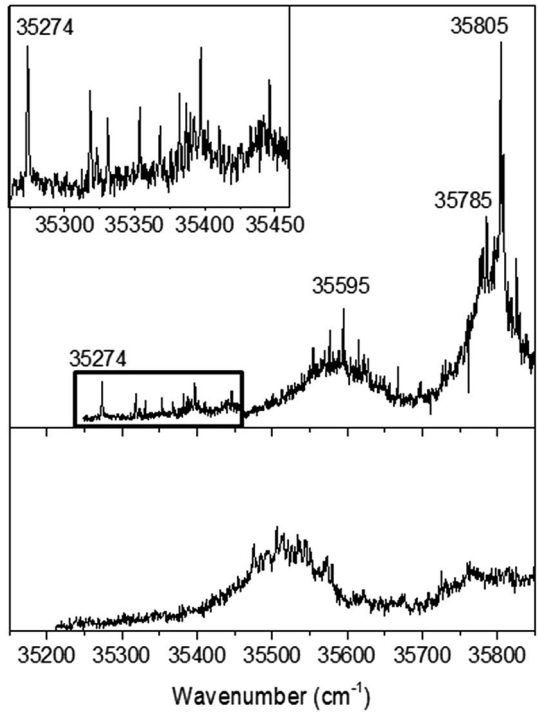

Fig. 8 S_0–S_1 electronic spectra of cyclo Tyr–Tyr: c-LL (top) and c-LD (bottom).

(b) Vibrational spectroscopy and assignment

c-LL. The double resonance spectrum of c-LL recorded setting the probe at the origin transition located at 35 274 cm^{-1} is shown in Fig. 9. The spectrum recorded by setting the probe at any of the other narrow transitions is identical to that taken at the origin. The probed conformer is called conformer $A_{c\text{-}LL}$ in what follows. The spectrum is divided into three regions. A narrow band appears at 3648 cm^{-1}, in the free ν(OH) stretching range. Second, an intense peak appears at 3554 cm^{-1}, in the range where bound ν(OH) stretches are expected. Lastly, a doublet appears at 3409 and 3428 cm^{-1}, in the ν(NH) stretching range.

The double resonance spectra of c-LL has also been recorded setting the probe on the two broad maxima. The obtained spectra are identical to each other but strongly differ from that obtained when probing the narrow transitions. This indicates that the broad absorption is due to a second conformer, denoted conformer $B_{c\text{-}LL}$ hereafter, or several conformers belonging to the same family and showing the same vibrational spectrum. A narrow band appears at 3656 cm^{-1}, in the free ν(OH) stretching range. A congested triplet appears in the region of the ν(NH) stretch, at 3400, 3412, and 3424 cm^{-1}.

Setting the IR probe at other characteristic transitions does not reveal new UV absorption, which unambiguously shows that all of the conformers have been detected.

c-LD. The double resonance spectra of c-LD recorded setting the probe at the two maxima of the broad absorption bands at 35 500 and 35 800 cm^{-1} are

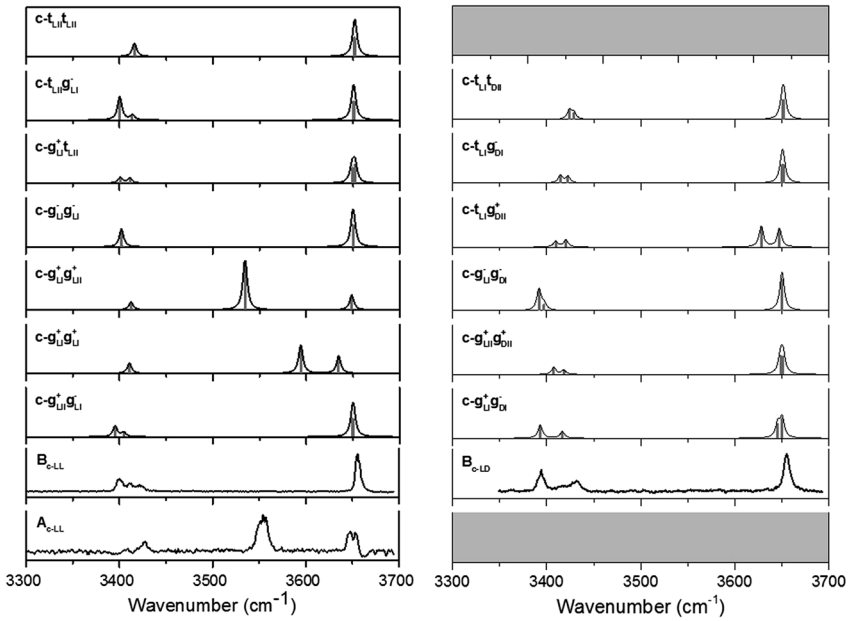

Fig. 9 Comparison between the experimental spectra of c-LL (left) and c-LD (right) and those calculated for the most stable structures of each calculated family. Note that the two most stable structures of c-$g_L^+g_L^+$ have been shown for c-LL (see text).

identical, as shown in Fig. 9. The obtained spectrum resembles that of conformer $B_{c\text{-}LL}$ of c-LL and the corresponding structure is called conformer $B_{c\text{-}LD}$. The spectrum is characterised by an intense band at 3655 cm^{-1} typical of a free ν(OH) stretch and, in the region of the ν(NH) stretch, a doublet at 3394/3432 cm^{-1} accompanied by a shoulder at 3417 cm^{-1}. Setting the IR probe to the most intense vibrational transition at 3655 cm^{-1} or at 3432 cm^{-1} and scanning the UV does not reveal new UV absorptions.

The two conformers of c-LL, $A_{c\text{-}LL}$ and $B_{c\text{-}LL}$, and the unique conformer $B_{c\text{-}LD}$ of c-LD, are assigned to calculated structures based on stability and agreement of experimental and simulated IR spectra. The vibrational pattern observed for conformer $B_{c\text{-}LL}$ is well reproduced by the spectrum of any of the structures of the most stable c-$g_L^+g_L^-$ family. The spectrum of conformer $B_{c\text{-}LL}$ is compared in Fig. 9 to the most stable of them, c-$g_{LII}^+g_{LI}^-$. The sharp band at 3656 cm^{-1} is a superposition of the two ν(OH) stretches, which are both completely free and are calculated at the same value. Two bands out of the triplet in the 3400/3412 cm^{-1} range can be safely assigned to two non-equivalent ν(NH) stretches, calculated at 3400 and 3411 cm^{-1} for the NH$\cdots\pi$ and free NH, respectively. The third one may be an overtone of the amide I or a combination band involving amides I and II. Other peptides, including DKP peptides, show such a combination or overtone band in this region.[30,75]

The spectrum of conformer $A_{c\text{-}LL}$ is well reproduced by that calculated for c-$g_{LI}^+g_{LII}^+$. The feature at 3648 cm^{-1} is assigned to the free ν(OH) calculated at 3649 cm^{-1}. The different structures belonging to the hydrogen-bonded c-$g_L^+g_L^+$ family do not have identical spectra. As mentioned above, c-$g_{LI}^+g_{LII}^+$ is stabilised

relative to the others because the relative position of the OH groups allows optimisation of their interaction. This is manifested by a larger red shift of the ν(OH) stretch in the vibrational spectrum of c-$g_{LI}{}^{+}g_{LII}{}^{+}$ relative to that of c-$g_{LI}{}^{+}g_{LI}{}^{+}$ or c-$g_{LII}{}^{+}g_{LII}{}^{+}$. Therefore, the feature at 3554 cm^{-1} in the spectrum of $A_{c\text{-}LL}$ unambiguously allows assignment of this conformer to c-$g_{LI}{}^{+}g_{LII}{}^{+}$. The band at 3409 cm^{-1} is assigned to the ν(NH) stretches calculated at 3413/3414 cm^{-1}. Interestingly, the calculated ν(NH) modes involve strongly coupled elongations of the two amide NH, which contrast with c-$g_{LII}{}^{+}g_{LI}{}^{-}$ or the parent cyclo Phe–Phe molecule in which they are well localised on each NH. The two frequencies observed here are thus the weak symmetric and strong antisymmetric stretches. Lastly, the band at 3428 cm^{-1} is assigned to an overtone or combination band.

We have checked the hypothesis that the additional band observed in the region of the ν(NH) stretches is an overtone or a combination band on the example of c-$g_{LI}{}^{+}g_{LII}{}^{+}$. Anharmonic frequencies, taking only a few relevant modes into account (OH and NH stretches as well as amide I and II) were computed for this structure using the variational perturbation theory.[76] The results are shown in Fig. S1 in the ESI.† As observed in parent cyclo Phe–Phe,[30] the overtone of the ν(CO) stretch (amide I) appears strongly in the calculations and could explain the experimental findings.

The assignment of $B_{c\text{-}LD}$ parallels that of $B_{c\text{-}LL}$. $B_{c\text{-}LD}$ is assigned to one or several members of the c-$g_{L}{}^{+}g_{D}{}^{-}$ family, on the basis of both stability and spectral similitude.

(c) Vibrational spectroscopy of the ion. The vibrational spectrum of the ion is recorded by setting the UV probe at the same wavelengths as for the neutral forms (see Fig. 10) and monitoring either the depletion of the parent at *m*/*z* 326 or of the increased intensity of the fragment at *m*/*z* 220 (cyclo Gly–Tyr radical cation), which corresponds to the loss of C_7H_6O. This corresponds to a neutral radical, either $^{\bullet}CHC_6H_4OH$ or $CH_2C_6H4O^{\bullet}$. Both structures correspond to the C_α–C_β cleavage, the former with concomitant H migration from the C_β carbon to the DKP ring, the latter from H transfer from the phenol hydroxyl. The spectra are identical whatever the position of the probe (broad features or, in the case of c-LL, narrow absorption bands), and whether the intensity of the parent or that of the fragment is monitored. Although they display some similitudes, the spectra of c-LL and c-LD slightly differ from each other. That of c-LD shows a transition in the same region as the free ν(OH) of the neutral ground state, at 3642 cm^{-1}. A second intense band appears more to the red region, at 3572 cm^{-1}. This value is slightly shifted up in energy relative to that measured in the hydrogen-bonded neutral c-$g_{LI}{}^{+}g_{LII}{}^{+}$ conformer (3554 cm^{-1}) or in the phenol/argon cation (3535 cm^{-1}).[77] Lastly, a weak band appears at 3410 cm^{-1}, in the region of the ν(NH) stretch of the neutral ground state. This spectrum agrees well with that simulated for c_{ion}-$g_{LI}{}^{+}t_{DI}$. In particular, the dissymmetry of the phenol rings, which was apparent from the charge distribution, is well reflected in the spectroscopy. The 3642 cm^{-1} transition is assigned to the free ν(OH) of the "neutral" $g_{LI}{}^{+}$ ring calculated at 3638 cm^{-1} while that at 3572 cm^{-1} is assigned to the free ν(OH) of the "charged" t_{DI} ring, calculated at 3586 cm^{-1}. This value is close to that observed in the radical cation of cyclo tyrosine–proline, where there is only one aromatic ring hence one possibility of charge localisation.[78] The 3410 cm^{-1} feature is assigned to the superposition of the two ν(NH) calculated at identical values (3400 cm^{-1}).

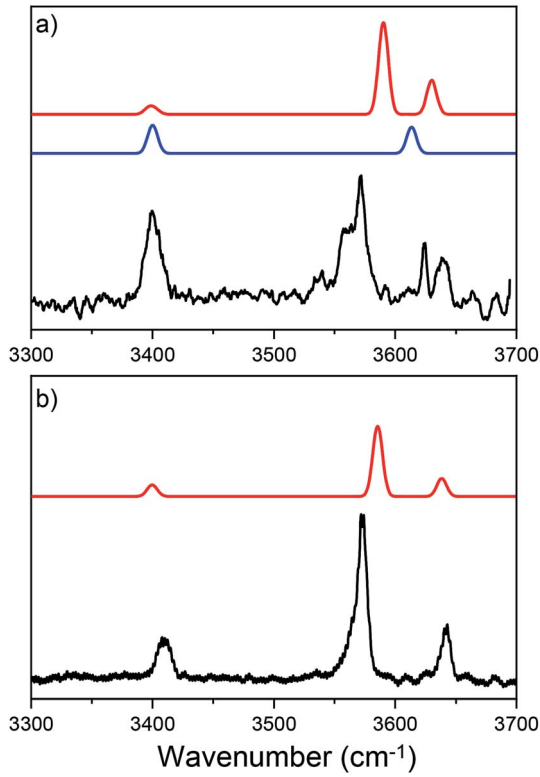

Fig. 10 Experimental and simulated spectra of the radical cation of (a) c-LL and (b) c-LD together with corresponding calculated structures. (a) c_{ion}-$g_{LII}^{+}t_{LII}$ (red) and c_{ion}-$g_{LI}^{+}g_{LII}^{+}$ (blue) and (b) c_{ion}-$g_{LI}^{+}t_{DI}$ (red).

The spectrum of c-LD can be tentatively explained in terms of the contributions of two structures, the first one being similar to that described for c-LD, namely, c_{ion}-$g_{LII}^{+}t_{LII}$. The weak band at 3635 cm^{-1} is the free ν(OH) of the "neutral" g_{LII}^{+} ring calculated at 3630 cm^{-1} while that at 3569 cm^{-1} is assigned to the free ν(OH) of the "charged" t_{LII} ring, calculated at 3590 cm^{-1}. The other calculated structure, c_{ion}-$g_{LI}^{+}g_{LI}^{+}$, can also contribute to the spectrum. The band at 3619 cm^{-1} could be assigned to its free ν(OH), calculated at 3613 cm^{-1}. It should be noted that the relative intensity of the band at 3394 cm^{-1} is larger than in the spectrum of c-LD. This could be explained if this band is assigned to the intense bound ν(OH) of c_{ion}-$g_{LI}^{+}g_{LI}^{+}$, calculated at 3399 cm^{-1}, superimposed with the ν(NH) stretches of c_{ion}-$g_{LII}^{+}t_{LII}$ and c_{ion}-$g_{LI}^{+}g_{LI}^{+}$, which are all calculated in this range. Lastly, one cannot exclude that the broader band appearing as a shoulder of the free ν(OH) stretch is a hot band, as already observed in photo-produced radical cations.[39]

The optically produced radical cation of c-LD evolves towards a well-defined geometry, while that of c-LL evolves to two different structures. Despite the fact that the c_{ion}-$g_{LII}^{+}t_{LII}$ structure with folded/extended rings is much less stable than the hydrogen-bonded c_{ion}-$g_{LI}^{+}g_{LI}^{+}$ form, there is spectroscopic evidence of its presence. Thus, energy redistribution in the ion populates the two forms.

(d) Localisation of the electronic energy. We can first compare cyclo Tyr–Tyr to tyrosine or tyrosine-containing peptides.[72,79] The 35 274 cm^{-1} band in the UV spectrum of c-LL is assigned to the origin transition of c-$g_{LI}^{+}g_{LII}^{+}$. This value is shifted down in energy relative to those observed in tyrosine itself, which range from 35 491 cm^{-1} to 35 650 cm^{-1} depending on the conformer.[72] It has been suggested that the origin of the tyrosine–glycine or tyrosine–glycine–glycine conformers is not much shifted relative to tyrosine, unless the hydroxyl group of tyrosine is involved in a strong interaction.[79] In this case, it is shifted down in energy by ~400 cm^{-1}. The fact that the origin of the hydrogen-bonded conformer of cLL, c-$g_{LI}^{+}g_{LII}^{+}$, is lower in energy than that of the other conformers agrees well with the previous experimental findings. We can also compare cyclo Tyr–Tyr to the previously studied cyclo Phe–Phe dipeptide.[30] In the latter, which is a c-$g^{+}g^{-}$ structure for both diastereomers, the first electronic transition is a $\pi\pi^*$ transition localised on the extended g^{-} aromatic ring, as it is in the c-$g^{+}g^{-}$conformers of cyclo Tyr–Tyr. Both experimental and theoretical results point out the localisation of the electronic excitation on one aromatic ring. Finally, we can compare the calculated transition energies to the experimental UV spectra. The order of the calculated S_0–S_1 transition energy is c-$g_{LI}^{+}g_{LII}^{+}$ < c-$g_{L}^{+}g_{D}^{-}$ < c-$g_{L}^{+}g_{L}^{-}$, which agrees well with the experimental findings.

IV. Conclusions

The spectroscopic results presented here indicate that a similar family of conformers exists in both systems, namely, c-$g_{L}^{+}g_{L}^{-}$ and c-$g_{L}^{+}g_{D}^{-}$. These conformers have one aromatic ring folded on the dipeptide DKP ring and the other one extended. This allows weak NH$\cdots\pi$ and CH$\cdots\pi$ interactions to take place. The NH… π interaction is slightly weaker in c-LL than c-LD. On the other hand, the CH$\cdots\pi$ interaction is slightly stronger in c-LD than in c-LL; it involves $C_\beta H$ in the later and $C_\alpha H$ in the former. This parallels the properties of the related cyclo Phe–Phe system, where the c-$g_{L}^{+}g_{L}^{-}$ or c-$g_{L}^{+}g_{D}^{-}$ geometries are the only ones observed.[30] In cyclo Phe–Phe, the stacked structure is much higher in energy because dispersion does not counterbalance repulsion. In contrast, in the system studied here, the tyrosine hydroxyls provide an additional anchoring site between the two aromatic rings. As a result, the stacked conformer c-$g_{LI}^{+}g_{LI}^{+}$ is stabilised. In c-LL, the L conformation of the two residues allows formation of a hydrogen bond. However, the red shift of the bound ν(OH) relative to the free ν(OH) stretch (94 cm^{-1}) is slightly weaker than that observed in the phenol dimer (124 cm^{-1}).[80] This is because the steric constraints brought by the DKP ring prevent the hydrogen bond from being optimal. Proper H-bonding interaction is not possible in the c-LD diastereomer and the c-$g_{L}^{+}g_{D}^{+}$ conformers are high in energy.

The solution-phase study of c-LL using electronic circular dichroism combined with molecular dynamics has suggested the coexistence of several conformers.[56] One of them is similar to the hydrogen-bonded c-$g_{LI}^{+}g_{LI}^{+}$ form that we have described in this work and the others belong to the c-$g_{L}^{+}g_{L}^{-}$ family. The related molecule cyclo Phe–Tyr has been studied using NMR spectroscopy.[47] The results suggest that the structure of cyclo LPhe–LTyr is similar to c-$g_{LI}^{+}g_{LI}^{+}$, in which the DKP ring is almost planar and the two aromatic rings share the space over the diketopiperazine ring in a face-to-face arrangement. For cyclo LPhe–DTyr, the NMR results suggest two conformations similar to c-$g_{L}^{+}g_{D}^{-}$ in terms of aromatic

ring arrangement. It would be interesting to study this system under supersonic expansion conditions to see whether the stabilisation of only c-$g_{LI}^{+}g_{LI}^{+}$ is possible.

Finally, it should be mentioned that the c-$g^{+}g^{-}$ structure seems to be the most stable one when no other interactions take place in the system, as observed in cyclo Phe–Phe, protonated cyclo Phe–Phe,[30,49] or cyclo LTyr–DTyr. Another structure is stabilised only if an additional interaction takes place between the two aromatic rings that is stronger than the CH$\cdots\pi$ interaction stabilising c-$g^{+}g^{-}$. In cyclo Tyr–Tyr, this interaction is an OH$\cdots$O hydrogen bond which is optimal only in c-LL. This explains the strong chirality-dependence of the structure observed here. This strong difference between the two forms is partly maintained in the ion, where the spectrum of c-LD is explained in terms of one structure only while that of c-LD might contain the signature of two conformers.

Conflicts of interest

There are no conflicts of interest to declare.

Acknowledgements

Support from the French National Research Agency (ANR) is acknowledged (Grant ANR-14-CE06-0019-03). We acknowledge the use of the computing facility cluster MésoLUM of the LUMAT federation (FR LUMAT 2764).

References

1 K. Schwing and M. Gerhards, *Int. Rev. Phys. Chem.*, 2016, **35**, 569–677.
2 E. Gloaguen and M. Mons, in *Gas-Phase IR Spectroscopy and Structure of Biological Molecules*, ed. A. M. Rijs and J. Oomens, 2015, vol. 364, pp. 225–270.
3 T. S. Zwier, *J. Phys. Chem. A*, 2006, **110**, 4133–4150.
4 R. J. Plowright, E. Gloaguen and M. Mons, *ChemPhysChem*, 2011, **12**, 1889–1899.
5 E. Gloaguen, Y. Loquais, J. A. Thomas, D. W. Pratt and M. Mons, *J. Phys. Chem. B*, 2013, **117**, 4945–4955.
6 Y. Loquais, E. Gloaguen, S. Habka, V. Vaquero-Vara, V. Brenner, B. Tardivel and M. Mons, *J. Phys. Chem. A*, 2015, **119**, 5932–5941.
7 M. Alauddin, E. Gloaguen, V. Brenner, B. Tardivel, M. Mons, A. Zehnacker-Rentien, V. Declerck and D. J. Aitken, *Chem.–Eur. J.*, 2015, **21**, 16479–16493.
8 W. H. James, E. E. Baquero, S. H. Choi, S. H. Gellman and T. S. Zwier, *J. Phys. Chem. A*, 2010, **114**, 1581–1591.
9 W. H. James III, E. G. Buchanan, C. W. Mueller, J. C. Dean, D. Kosenkov, L. V. Slipchenko, L. Guo, A. G. Reidenbach, S. H. Gellman and T. S. Zwier, *J. Phys. Chem. A*, 2011, **115**, 13783–13798.
10 W. H. James, E. G. Buchanan, C. W. Mueller, T. S. Zwier, S. H. Choi, L. Guo and S. H. Gellman, *Abstracts of Papers of the American Chemical Society*, 2011, vol. 241.
11 R. Kusaka, D. Zhang, P. S. Walsh, J. R. Gord, B. F. Fisher, S. H. Gellman and T. S. Zwier, *J. Phys. Chem. A*, 2013, **117**, 10847–10862.
12 P. S. Walsh, R. Kusaka, E. G. Buchanan, W. H. James III, B. F. Fisher, S. H. Gellman and T. S. Zwier, *J. Phys. Chem. A*, 2013, **117**, 12350–12362.

13 K. Schwing, C. Reyheller, A. Schaly, S. Kubik and M. Gerhards, *ChemPhysChem*, 2011, **12**, 1981–1988.
14 S. Ishiuchi, K. Yamada, H. Oba, H. Wako and M. Fujii, *Phys. Chem. Chem. Phys.*, 2016, **18**, 23277–23284.
15 N. J. Zondlo, *Acc. Chem. Res.*, 2013, **46**, 1039–1049.
16 S. Tsuzuki and A. Fujii, *Phys. Chem. Chem. Phys.*, 2008, **10**, 2584–2594.
17 S. Tsuzuki, K. Honda, T. Uchimaru, M. Mikami and K. Tanabe, *J. Am. Chem. Soc.*, 2000, **122**, 11450–11458.
18 R. N. Pribble and T. S. Zwier, *Science*, 1994, **265**, 75–79.
19 S. Y. Fredericks, K. D. Jordan and T. S. Zwier, *J. Phys. Chem.*, 1996, **100**, 7810–7821.
20 N. Seurre, J. Sepiol, F. Lahmani, A. Zehnacker-Rentien and K. Le Barbu-Debus, *Phys. Chem. Chem. Phys.*, 2004, **6**, 4658–4664.
21 W. Y. Sohn, V. Brenner, E. Gloaguen and M. Mons, *Phys. Chem. Chem. Phys.*, 2016, **18**, 29969–29978.
22 H. S. Biswal, E. Gloaguen, Y. Loquais, B. Tardivel and M. Mons, *J. Phys. Chem. Lett.*, 2012, **3**, 755–759.
23 D. Scuderi, K. Le Barbu-Debus and A. Zehnacker, *Phys. Chem. Chem. Phys.*, 2011, **13**, 17916–17929.
24 W. H. James III, E. G. Buchanan, L. Guo, S. H. Geman and T. S. Zwier, *J. Phys. Chem. A*, 2011, **115**, 11960–11970.
25 A. Stamm, D. Bernhard and M. Gerhards, *Phys. Chem. Chem. Phys.*, 2016, **18**, 15327–15336.
26 G. B. McGaughey, M. Gagne and A. K. Rappe, *J. Biol. Chem.*, 1998, **273**, 15458–15463.
27 S. K. Burley and G. A. Petsko, *Science*, 1985, **229**, 23–28.
28 A. G. Abo-Riziq, J. E. Bushnell, B. Crews, M. P. Callahan, L. Grace and M. S. de Vries, *Int. J. Quantum Chem.*, 2005, **105**, 437–445.
29 E. Gloaguen, H. Valdes, F. Pagliarulo, R. Pollet, B. Tardivel, P. Hobza, F. Piuzzi and M. Mons, *J. Phys. Chem. A*, 2010, **114**, 2973–2982.
30 A. Perez-Mellor, I. Alata, V. Lepère and A. Zehnacker, *J. Mol. Spectrosc.*, **2018**, 71–84.
31 R. C. Dunbar, J. D. Steill and J. Oomens, *J. Am. Chem. Soc.*, 2011, **133**, 1212–1215.
32 V. Lepere, K. Le Barbu-Debus, C. Clavaguera, D. Scuderi, G. Piani, A.-L. Simon, F. Chirot, L. MacAleese, P. Dugourd and A. Zehnacker, *Phys. Chem. Chem. Phys.*, 2016, **18**, 1807–1817.
33 H. C. Gottschalk, A. Poblotzki, M. A. Suhm, M. M. Al-Mogren, J. Antony, A. A. Auer, L. Baptista, D. M. Benoit, G. Bistoni, F. Bohle, R. Dahmani, D. Firaha, S. Grimme, A. Hansen, M. E. Harding, M. Hochlaf, C. Holzer, G. Jansen, W. Klopper, W. A. Kopp, L. C. Kroger, K. Leonhard, H. Mouhib, F. Neese, M. N. Pereira, I. S. Ulusoy, A. Wuttke and R. A. Mata, *J. Chem. Phys.*, 2018, **148**, 014301.
34 J. Altnoeder, A. Bouchet, J. J. Lee, K. E. Otto, M. A. Suhm and A. Zehnacker-Rentien, *Phys. Chem. Chem. Phys.*, 2013, **15**, 10167–10180.
35 T. van Mourik, *J. Chem. Theory Comput.*, 2008, **4**, 1610–1619.
36 A. Sen, A. Bouchet, V. Lepere, K. Le Barbu-Debus, D. Scuderi, F. Piuzzi and A. Zehnacker-Rentien, *J. Phys. Chem. A*, 2012, **116**, 8334–8344.

37 A. Sen, V. Lepere, K. Le Barbu-Debus and A. Zehnacker, *ChemPhysChem*, 2013, **14**, 3559–3568.
38 J. C. Dean, E. G. Buchanan, W. H. James, A. Gutberlet, B. Biswas, P. V. Ramachandran and T. S. Zwier, *J. Phys. Chem. A*, 2011, **115**, 8464–8478.
39 A. Mahjoub, A. Chakraborty, V. Lepere, K. Le Barbu-Debus, N. Guchhait and A. Zehnacker, *Phys. Chem. Chem. Phys.*, 2009, **11**, 5160–5169.
40 M. E. Crestoni, B. Chiavarino, D. Scuderi, A. Di Marzio and S. Fornarini, *J. Phys. Chem. B*, 2012, **116**, 8771–8779.
41 A. Bouchet, J. Klyne, G. Piani, O. Dopfer and A. Zehnacker, *Phys. Chem. Chem. Phys.*, 2015, **17**, 25809–25821.
42 E. Gloaguen, F. Pagliarulo, V. Brenner, W. Chin, F. Piuzzi, B. Tardivel and M. Mons, *Phys. Chem. Chem. Phys.*, 2007, **9**, 4491–4497.
43 W. H. James III, E. E. Baquero, V. A. Shubert, S. H. Choi, S. H. Gellman and T. S. Zwier, *J. Am. Chem. Soc.*, 2009, **131**, 6574–6590.
44 Y. P. Hong, S. H. Lee, J. H. Choi, A. Kashima, G. Nakamura and T. Suzuki, *Bull. Kor. Chem. Soc.*, 2014, **35**, 2299–2303.
45 P. J. Milne, A. L. Hunt, K. Rostoll, J. J. Van Der Walt and C. J. Graz, *J. Pharm. Pharmacol.*, 1998, **50**, 1331–1337.
46 G. Kilian, H. Jamie, S. C. A. Brauns, K. Dyason and P. J. Milne, *Pharmazie*, 2005, **60**, 305–309.
47 T. Yamazaki, K. I. Nunami and M. Goodman, *Biopolymers*, 1991, **31**, 1513–1528.
48 S. Wiedemann, A. Metsala, D. Nolting and R. Weinkauf, *Phys. Chem. Chem. Phys.*, 2004, **6**, 2641–2649.
49 I. Alata, A. Perez-Mellor, F. Ben Nasr, D. Scuderi, V. Steinmetz, F. Gobert, N. E. Jaidane and A. Zehnacker-Rentien, *J. Phys. Chem. A*, 2017, **121**, 7130–7138.
50 E. Gross, *The Peptides Analysis, Synthesis, Biology: Modern Techniques of Conformational Structural, and Configurational Analysis*, Elsevier, 2012.
51 K. L. Carlson, S. L. Lowe, M. R. Hoffmann and K. A. Thomasson, *J. Phys. Chem. A*, 2005, **109**, 5463–5470.
52 P. J. Milne, D. W. Oliver and H. M. Roos, *J. Crystallogr. Spectrosc. Res.*, 1992, **22**, 643–649.
53 E. Sletten, *J. Am. Chem. Soc.*, 1970, **92**, 172–177.
54 M. Gdaniec and B. Liberek, *Acta Crystallogr. Sect. C Cryst. Struct. Commun.*, 1986, **42**, 1343–1345.
55 K. D. Kopple and D. H. Marr, *J. Am. Chem. Soc.*, 1967, **89**, 6193–6200.
56 J. Fleischhauer, J. Grotzinger, B. Kramer, P. Kruger, A. Wollmer, R. W. Woody and E. Zobel, *Biophys. Chem.*, 1994, **49**, 141–152.
57 E. T. Mengesha, A. Zehnacker-Rentien, J. Sepiol, M. Kijak and J. Waluk, *J. Phys. Chem. B*, 2015, **119**, 2193–2203.
58 C. Riehn, C. Lahmann, B. Wassermann and B. Brutschy, *Chem. Phys. Lett.*, 1992, **197**, 443–450.
59 S. Tanabe, T. Ebata, M. Fujii and N. Mikami, *Chem. Phys. Lett.*, 1993, **215**, 347–352.
60 M. D. Halls, J. Velkovski and H. B. Schlegel, *Theor. Chem. Acc.*, 2001, **105**, 413.
61 S. Grimme, J. Antony, S. Ehrlich and H. Krieg, *J. Chem. Phys.*, 2010, **132**, 154104.
62 S. Grimme, S. Ehrlich and L. Goerigk, *J. Comput. Chem.*, 2011, **32**, 1456–1465.

63 A. E. Reed, L. A. Curtiss and F. Weinhold, *Chem. Rev.*, 1988, **88**, 899–926.
64 M. J. Frisch, G. W. Trucks, H. B. Schlegel, G. E. Scuseria, M. A. Robb, J. R. Cheeseman, G. Scalmani, V. Barone, B. Mennucci, G. A. Petersson, H. Nakatsuji, M. Caricato, X. J. Li, H. P. Hratchian, A. F. Izmaylov, J. Bloino, G. Zheng, J. L. Sonnenberg, M. Hada, M. Ehara, K. Toyota, R. Fukuda, J. Hasegawa, M. Ishida, T. Nakajima, Y. Honda, O. Kitao, H. Nakai, T. Vreven, J. A. Montgomery Jr, J. E. Peralta, F. Ogliaro, M. Bearpark, J. J. Heyd, E. Brothers, K. N. Kudin, V. N. Staroverov, R. Kobayashi, J. Normand, K. Raghavachari, A. Rendell, J. C. Burant, S. S. Iyengar, J. Tomasi, M. Cossi, N. Rega, J. M. Millam, M. Klene, J. E. Knox, J. B. Cross, V. Bakken, C. Adamo, J. Jaramillo, R. Gomperts, R. E. Stratmann, O. Yazyev, A. J. Austin, R. Cammi, C. Pomelli, J. W. Ochterski, R. L. Martin, K. Morokuma, V. G. Zakrzewski, G. A. Voth, P. Salvador, J. J. Dannenberg, S. Dapprich, A. D. Daniels, O. Farkas, J. B. Foresman, J. V. Ortiz, J. Cioslowski and D. J. S. Fox, *Gaussian 09, Revision A.02*, Gaussian Inc., Wallingford CT, 2009.
65 J. D. Chai and M. Head-Gordon, *Physical Chemistry Chemical Physics*, 2008, **10**, 6615–6620.
66 D. Jacquemin, E. A. Perpete, I. Ciofini and C. Adamo, *Theoretical Chemistry Accounts*, 2011, **128**, 127–136.
67 E. R. Johnson, S. Keinan, P. Mori-Sanchez, J. Contreras-Garcia, A. J. Cohen and W. Yang, *J. Am. Chem. Soc.*, 2010, **132**, 6498–6506.
68 J. Contreras-Garcia, W. T. Yang and E. R. Johnson, *J. Phys. Chem. A*, 2011, **115**, 12983–12990.
69 R. Chaudret, B. d. Courcy, J. Contreras-Garcia, E. Gloaguen, A. Zehnacker-Rentien, M. Mons and J. P. Piquemal, *Phys. Chem. Chem. Phys.*, 2014, **16**, 9876–9891.
70 W. Humphrey, A. Dalke and K. Schulten, *J. Mol. Graphics*, 1996, **14**, 33–38.
71 Y. Inokuchi, Y. Kobayashi, T. Ito and T. Ebata, *J. Phys. Chem. A*, 2007, **111**, 3209–3215.
72 Y. Shimozono, K. Yamada, S.-i. Ishiuchi, K. Tsukiyama and M. Fujii, *Phys. Chem. Chem. Phys.*, 2013, **15**, 5163–5175.
73 O. V. Boyarkin, S. R. Mercier, A. Kamariotis and T. R. Rizzo, *J. Am. Chem. Soc.*, 2006, **128**, 2816–2817.
74 S. Ishiuchi, H. Wako, D. Kato and M. Fujii, *J. Mol. Spectrosc.*, 2017, **332**, 45–51.
75 M. Gerhards and C. Unterberg, *Phys. Chem. Chem. Phys.*, 2002, **4**, 1760–1765.
76 J. Bloino and V. Barone, *J. Chem. Phys.*, 2012, **136**, 124108.
77 A. Pérez Mellor, I. Alata and A. Zehnacker, manuscript in preparation.
78 A. Fujii, T. Sawamura, S. Tanabe, T. Ebata and N. Mikami, *Chem. Phys. Lett.*, 1994, **225**, 104–107.
79 A. Abo-Riziq, L. Grace, B. Crews, M. P. Callahan, T. van Mourik and M. S. de Vries, *J. Phys. Chem. A*, 2011, **115**, 6077–6087.
80 T. Ebata, T. Watanabe and N. Mikami, *J. Phys. Chem.*, 1995, **99**, 5761–5764.